Modelling petroleum expulsion in sedimentary basins: the importance of igneous intrusion timing and basement composition

David Gardiner, Nick Schofield, Alex Finlay, Niall Mark, Liam Holt, Clayton Grove, Chris Forster & Julian Moore

SUPPLEMENTARY MATERIAL

The following material is provided to substantiate statements within the main paper and provide additional information on the modelling inputs, workflow and rationale.

Geochemical database

A comprehensive geochemical database has been compiled from existing regional studies (e.g. APT, 2017) and supplemented with more local, detailed data for the Cambo-Rosebank area. The total database comprises 1,292 samples from 36 wells, composed of 893 rock, 98 oil/stain and 301 gas samples.

Source rock characterization

The primary source rock intervals in the FSB are the Tithonian to Berriasian shales of the Kimmeridge Clay Formation (KCF). The lithology and geochemical properties are consistent with deposition in a low to moderate energy marine environment.

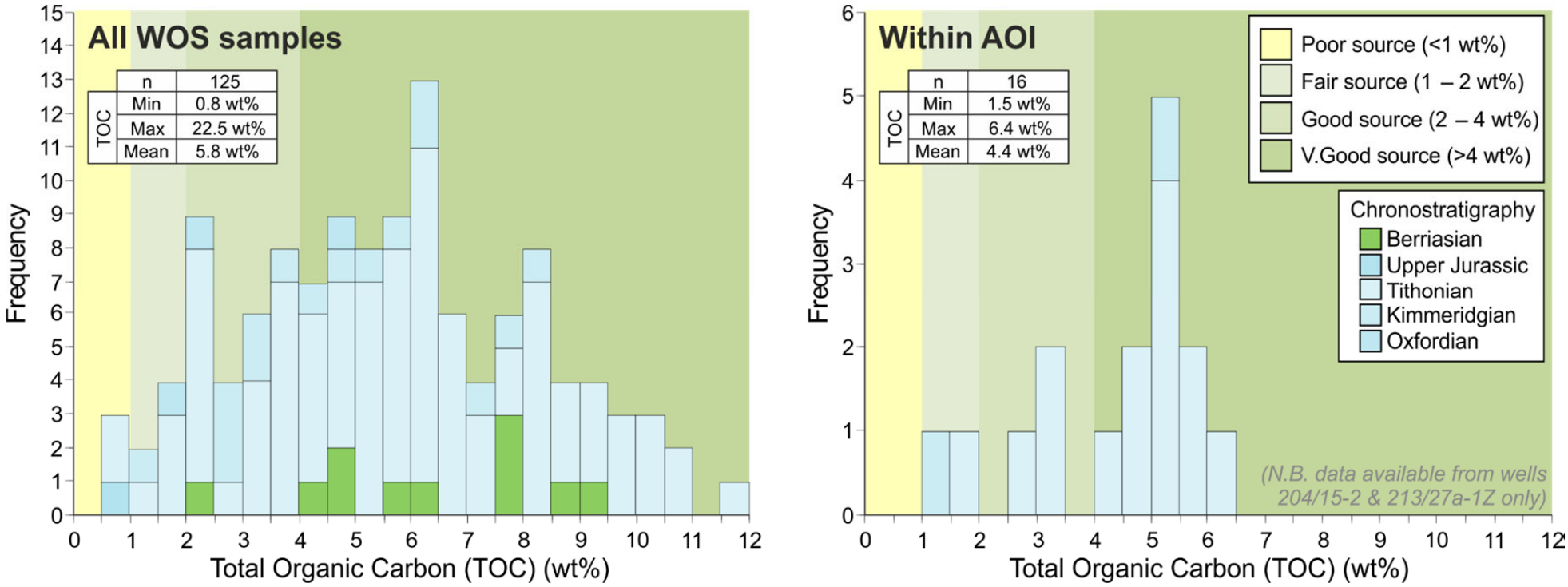

Total Organic Carbon (TOC) histograms of all Kimmeridge Clay Formation (KCF) rock samples within the whole West of Shetlands (WOS) database (left) and within the AOI only (right), with data taken from APT (2017) and plotted in *p:IGI-3*. The normal distribution of TOC samples regionally and mean value of 5.8 wt.% TOC indicates a world-class source rock, while the log-normal distribution and mean TOC of 4.4 wt.% in the smaller AOI suggests a slightly poorer, but still very good, clastic source rock.

All source rock volumetrics within the paper maintain source rock properties for consistency, using average values within the AOI. TOC of 4.4 wt.%; HI of 350 mg/gTOC; 100% Type II kerogen (Pepper & Corvi (1995) Organofacies B, marine clay-rich); thickness 100 m (except where eroded on Corona Ridge).

Oil geochemistry

Some of the key correlation characteristics between KCF source extracts and oils include a narrow range of isotopically-light carbon isotope values between $\delta^{13}C_{sats}$ of -31 to -30 ‰ & $\delta^{13}C_{arom}$ of -30.5 to -29.5 ‰, relatively high C_{27}/C_{29} αββ-steranes, relatively low C_{29}/C_{30} αβ-hopanes, low pristane/phytane (<1.5) and the presence of 28,30-bisnorhopane (often abundant).

The bacterial consumption of oils by bacteria (biodegradation) has significantly altered most oils within the FSB to varying degrees, which, combined with the evidence of charge mixing from the oil maturity, complicates the interpretation. The presence of 25-norhopanes within most samples indicates that oils have been severely biodegraded to an extent that would typically remove all *n*-alkanes and alter most saturate biomarkers (although aromatic biomarkers may be less affected) (Larter *et al.,* 2012). Therefore, the paradoxical presence of *n*-alkanes *and* 25-norhopanes must likely result from a mixture of severely biodegraded and fresher, non-altered oil. This may result from a severely biodegraded oils mixing with a more recent phase of charge which (re-)supplied *n*-alkanes either during migration or in the reservoir.

Together this implies that the oils are most likely comprised of a mixture of charge "pulses" from the same (or similar) source rock, but with slightly differing maturities based on the biomarker evidence.

Integrating this information with the basin modelling, the predicted reservoir temperature history, KCF charge "pulse" timing and estimated rate of biodegradation in the Cambo-Rosebank Paleogene reservoirs (from *Trinity T3*) infers that the most recent phase of oil charge must have occurred within the last 10 to 20 Myr, resulting in a predicted present-day oil density of *ca.* 32 °API (measured oil samples range from 25 – 38 °API). This evidence of recent charge

of fresh oil invokes some sort of "Motel Theory" (as discussed in the main article) and is the most probable timing for the (re-)supply of *n*-alkanes.

Considering total charge through time results in a predicted *increase* in oil density to *ca.* 15 °API. This is most likely due to the long residency time of oil in a low temperature (<80 °C) reservoir which is vulnerable to biodegradation. In this scenario the significant biodegradation (up to 70 % mass degradation) may be enough to produce the 25-norhopanes observed in the Cambo and Rosebank oils.

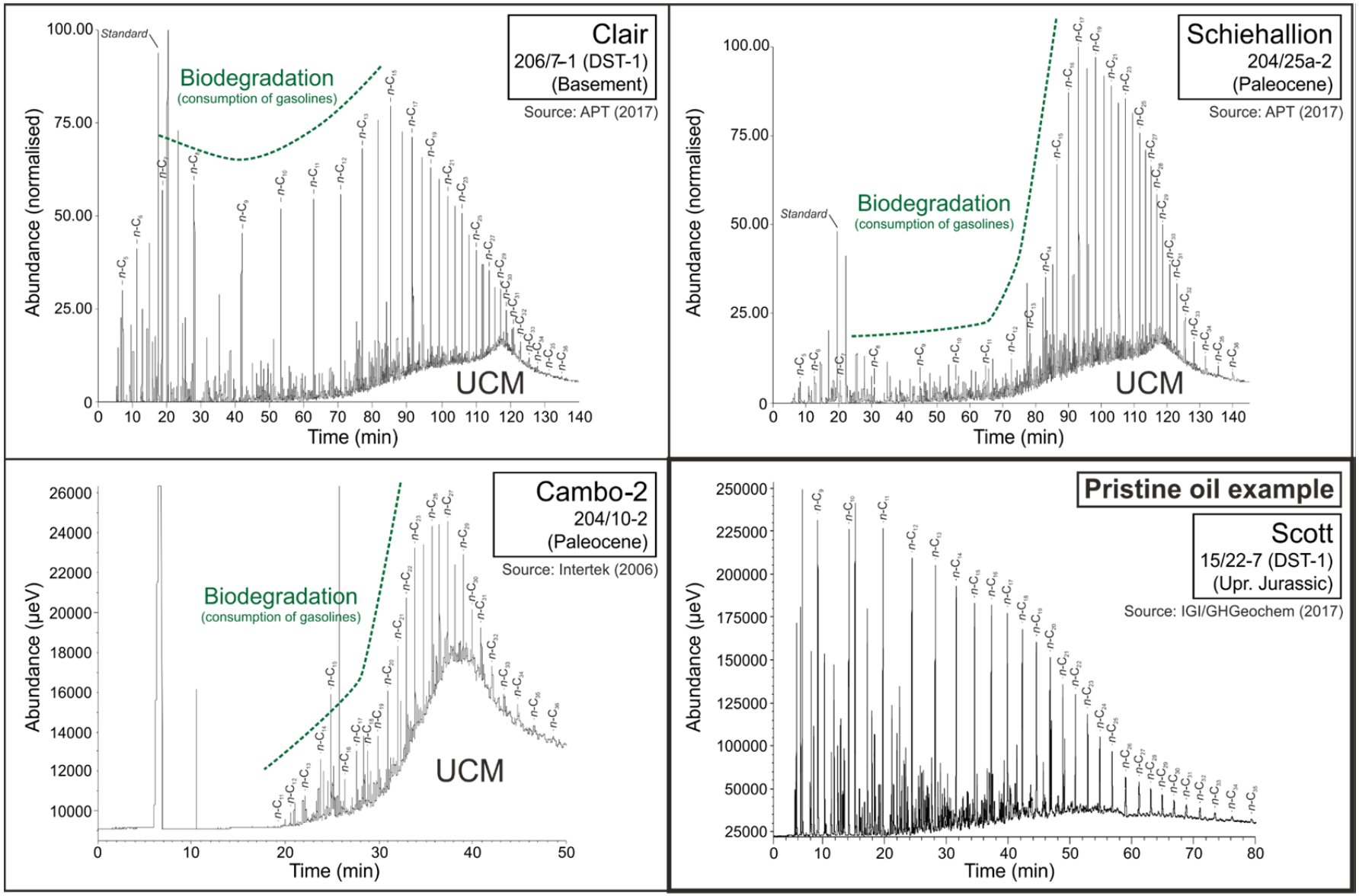

Whole-Oil Gas Chromatograms (WOGC) for 3 oil samples from the Cambo, Clair & Schiehallion fields in the FSB in comparison to a pristine oil from the North Sea (Scott field). Most FSB oils have a pronounced Unresolved Complex Mixture (UCM) and the presence of 25-Norhopanes (not shown, from GC-MS analysis), indicative of moderate and severe biodegradation, respectively. 25-Norhopanes are thought to be produced only under severe biodegradation, at which point all *n*-alkanes should be consumed/absent (Larter *et al.,* 2012). Therefore, the presence of *n*-alkanes (carbon numbers labelled in italics) in oils indicates some fresh re-supply/charge after this severe biodegradation has occurred. Subsequent moderate biodegradation has altered this fresh charge, consuming the gasoline-range *n*-alkanes (or removing them altogether e.g. Cambo).

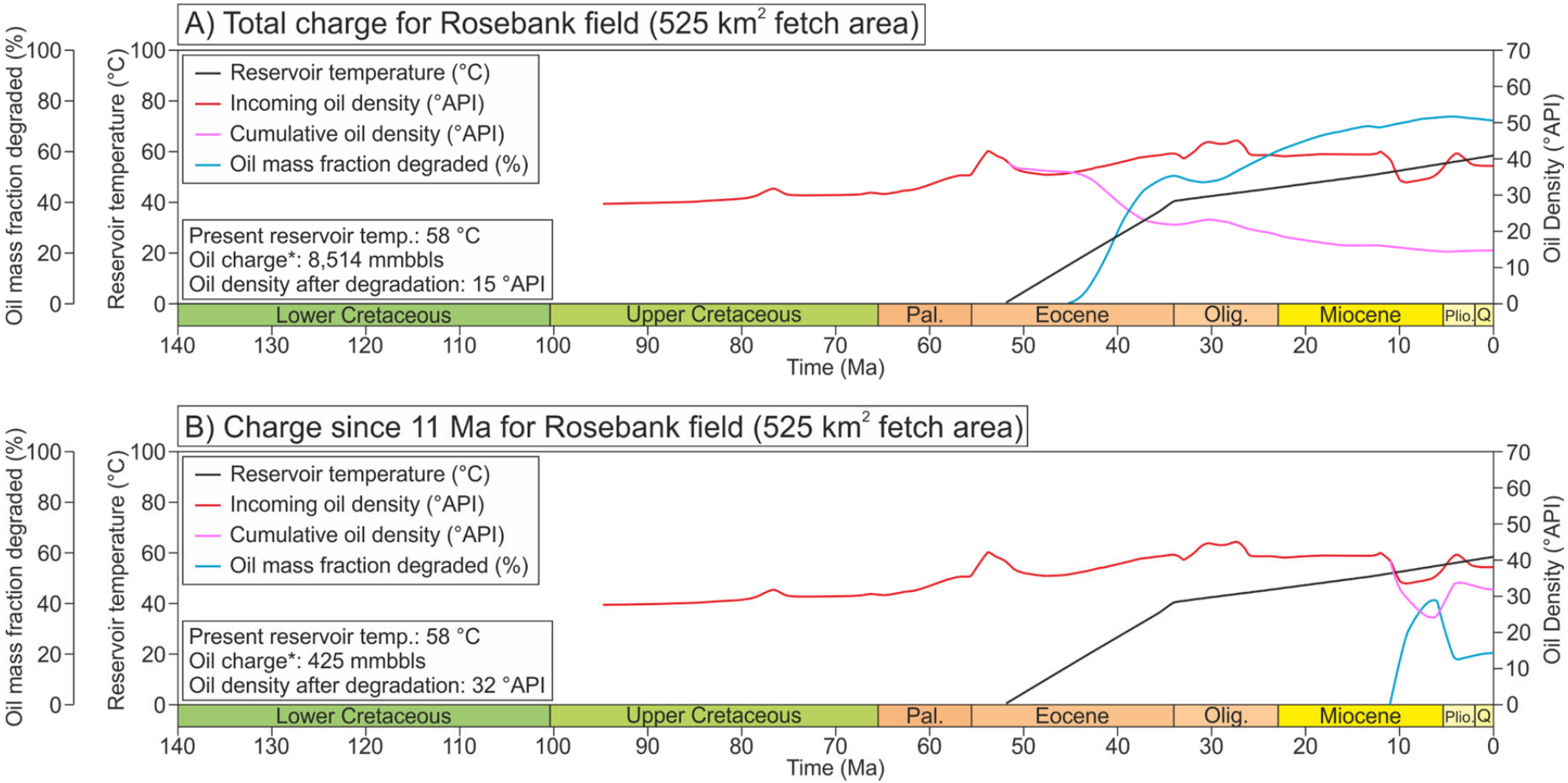

Integrated Eocene reservoir temperature and charge volume history for the Rosebank field on the Corona Ridge, produced using *Trinity T3*. The model includes both igneous intrusions "overthickening" and "Cold" RHP crustal model, varying only the charge timing. Scenario a) the total charge volume of oil and gas in the calculated 525 km² fetch area from the KCF source rock and b) the same KCF source rock and fetch area but considering charge since 11 Ma only. The comparison highlights that considering total charge results in a high oil density (low °API gravity) due to significant biodegradation (up to 70% mass degradation) associated with the low reservoir temperatures, perhaps severe enough to produce the 25-norhopanes observed in oils. Oil charge from 11 Ma occurs when the reservoir is hotter (less vulnerable to biodegradation) and in sufficient volumes to result in a cumulative oil density of a predicted 32 °API, which may be the source of more recent (re-) supply of *n*-alkanes observed in the oils regionally.

*KCF source rock properties (based on average values within the AOI): TOC of 4.4 wt.%; HI of 350 mg/gTOC; 100% Type II kerogen (Pepper & Corvi (1995) Organofacies B, marine clay-rich); thickness 100 m (except where eroded on Corona Ridge).

Calculating Radioactive Heat Production (RHP)

There are multiple methods of calculating RHP from elemental data assuming a rock density of 2,700 kg/m^3. In this study we compare two separate methods:

1. Rybach (1988) which models RHP based on U, Th & K

2. Turocotte & Schubert (2014) which considers the ^{238}U separately from ^{235}U.

Data for calculating RHP has been taken from Chemostrat's *West of Shetland Geochemical Database* and Chambers *et al.* (2005) and is presented in the table below. As demonstrated by Finlay (2019), RHP calculated by the two separate methods are indistinguishable. Interestingly, the mean RHP values are similar to the RHP value of onshore Lewisian outcrop samples (1.8 μW/m^3) presented by Khutorskoi & Polyak (2016).

Well	Depth (m)	Source	U (ppm)	Th (ppm)	K (ppm)	H (μW/m^3)	
						Rybach (1988)	Turocotte & Schubert (2014)
204/10-1	2,499.0	Chemostrat commercial data	3.17	1.58	20701	1.1	1.1
214/9-1	4,749.0	Chemostrat commercial data	7.92	1.51	38466	2.5	2.5
205/16-1	4,172.2	Chambers *et al.* (2005)	0.54	10.9	31296	1.2	1.2
					Mean	1.6	1.6
					S.D.	0.8	0.8

RHP data and calculations (assuming ρ = 2,700 kg/m^3) for samples in this study.

Basin modelling inputs and rationale

Stratigraphy

16 1-D models for exploration, appraisal and development wells were constructed to test the thermal and loading effects of igneous intrusions and the composition of basement rocks on source rock maturity across the *ca.*24,000 km^2 Area of Interest (AOI) (Figure 1 of the main article). The stratigraphic tops have been taken from completion logs and reports provided by the operator of the wells, with subsequent refinement based on separate biostratigraphic and chemostratigraphic commercial studies.

14 1-D pseudowells ("PW") have been constructed in key undrilled locations across the AOI, within the center of source rock kitchens (e.g. PW-1, PW-5) and on the flanks of the basin (e.g. PW-8, PW-10). The stratigraphic tops for the 1-D pseudowells and the grid-based 3-D model are constrained by the well-tied seismic interpretation, providing the depths of nine litho- and chrono-stratigraphic depth surfaces. These are (in increasing age):

1. Seafloor (0 Ma)
2. Top Miocene (5.3 Ma)
3. Top Eocene (33.9 Ma)
4. Top Paleocene (top igneous material) (55 Ma)
5. Top mid Paleocene (base igneous material) (58 Ma)
6. Top Upper Cretaceous (66 Ma)
7. Top Lower Cretaceous (100.5 Ma)
8. Top Kimmeridgian (152.1 Ma)
9. Top basement (2.7 Ga)

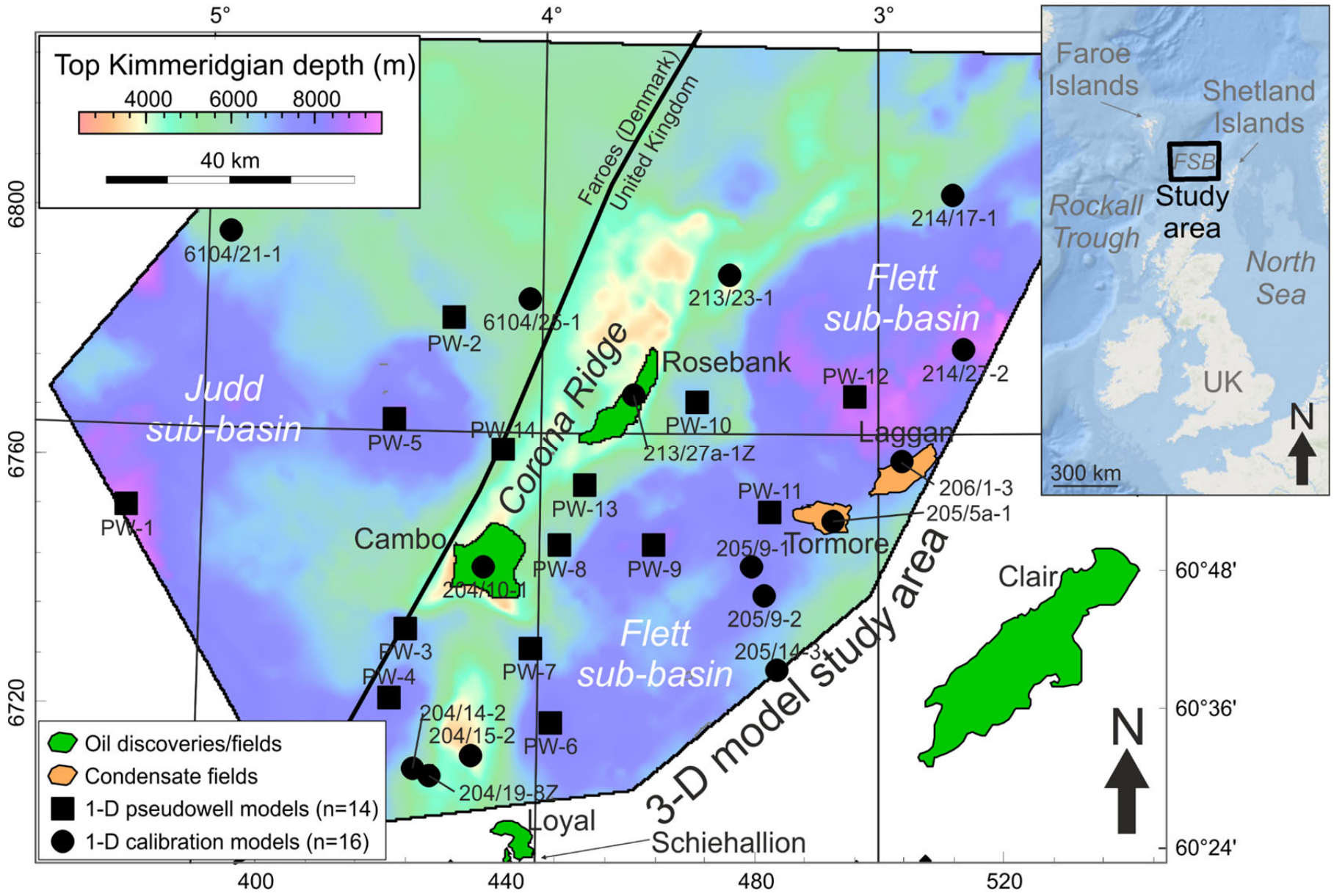

Top Kimmeridgian source rock depth map (m) from derived from seismic interpretation, including the Judd and Flett sub-basins and Corona Ridge, showing location of 1D calibration and pseudowell ("PW") models. NOTE: model 6004/14-1 is located behind the key in the bottom left corner.

Well or Pseudowell	Location		Base of model	Oldest lithostratigraphy	Oldest chronostratigraphy	Number of calibration data	
	Long (Dec)	Lat (Dec)	(mTVDSS)			Vitrinite reflectance	Temperature
204/10-1	-4.16	60.80	2,487.0	Basement	Archean	74	34
204/14-2	-4.36	60.51	4,236.7	T22 sandstone	Paleocene	6	3
204/15-2	-4.19	60.53	3,799.9	Basement	Archean	2	2
204/19-8Z	-4.31	60.50	4,168.0	T22 sandstone	Paleocene	43	7
205/5a-1	-3.14	60.87	3,937.0	Vaila Fm.	Paleocene	0	1
205/9-1	-3.37	60.81	4,724.1	Shetland Gp.	Upper Cretaceous	0	3
205/9-2	-3.33	60.77	3,857.4	T28 shale	Paleocene	0	1
205/14-3	-3.30	60.66	3,090.7	Jorsalfare Fm.	Upper Cretaceous	0	1
206/1-3	-2.93	60.96	4,714.5	Jorsalfare Fm.	Upper Cretaceous	0	3
213/23-1	-3.44	61.23	4,572.0	Basement	Archean	54	7
213/27a-1Z	-3.73	61.05	3,669.0	Clair Gp.	Devonian	25	1
214/17-1	-2.78	61.34	2,698.4	Eocene sandstone	Eocene	11	4
214/27-2	-2.75	61.12	4,429.0	Faroe Gp.	Paleocene	16	3
6004/17-1	-4.79	60.50	3,847.0	Vaila Fm.	Paleocene	0	1
6104/21-1	-4.93	61.28	4,225.0	Lamba Fm.	Paleocene	23	1
6104/25-1	-4.04	61.19	2,984.0	Lamba Fm.	Paleocene	5	2
PW-1	-4.43	61.01	8,989.3	Basement	Archean	-	-
PW-2	-4.26	61.16	8,566.0	Basement	Archean	-	-
PW-3	-4.39	60.71	8,137.0	Basement	Archean	-	-
PW-4	-4.43	60.61	8,591.1	Basement	Archean	-	-
PW-5	-5.22	60.88	10,129.3	Basement	Archean	-	-
PW-6	-3.96	60.58	8,400.0	Basement	Archean	-	-
PW-7	-4.02	60.69	7,422.8	Basement	Archean	-	-
PW-8	-3.94	60.84	6,715.5	Basement	Archean	-	-
PW-9	-3.66	60.84	8,628.4	Basement	Archean	-	-
PW-10	-3.54	61.04	8,850.9	Basement	Archean	-	-
PW-11	-3.32	60.88	8,924.5	Basement	Archean	-	-
PW-12	-3.07	61.05	9,658.8	Basement	Archean	-	-
PW-13	-3.87	60.92	6,835.7	Basement	Archean	-	-
PW-14	-4.11	60.97	7,262.7	Basement	Archean	-	-

Summary of 1-D modelling inputs, including location, stratigraphy and calibration data. Stratigraphic data for calibration wells are captured from completion logs and reports and pseudowell tops are captured from seismic data and lithological data from the most proximal calibration well. All models are created in ZetaWare Inc. *Genesis* software (v.5.8).

Thermal calibration

A transient, fixed temperature (1330 °C) full lithosphere thermal model has been used in all 1-D models and to under-pin the grid-based 3-D model (using temperature scaler maps of 1-D models). The 1330 °C-isotherm which marks a thermo-physical boundary between the lithospheric mantle and asthenosphere varies in depth in response to geological events; for example, uplift infers a shallowing of the lithosphere which brings the 1330 °C-isotherm closer to the surface, resulting in an increase in geothermal gradient and thus basal heat flow (depending on the erosion rate and magnitude).

The crustal structure in Genesis requires a thickness and composition for the upper crust, lower crust and lithospheric mantle. The crustal structure is based upon the work of Rippington *et al.* (2015), which utilizes gravity and magnetic data in conjunction with seismic data to map the sub-basalt structure of the FSB and model the crustal architecture of this part of the Atlantic margin. Using a transect of the crustal architecture of the FSB by Rippington *et al.* (2015), 1-D models have each been assigned variable thickness for each lithospheric interval, depending on the location within the basin or structural highs. These values have then been adjusted to thermally-calibrate to temperature and vitrinite reflectance data in each well location, generally with a good agreement.

The lithospheric structure in pseudowell locations uses the same methodology, but without calibration data, is adjusted based on any tweaks required by proximal drilled well 1-D models to match calibration data.

With the lithospheric component thicknesses set in each model, two thermal scenarios have been tested to compare the effect of basement (crustal) composition by varying the radiogenic heat production (RHP):

- "Warm" or "Typical" RHP model: upper crust heat production typical of North Sea (2.8 $\mu W/m^3$). This achieves good calibration to both temperature and maturity data but invokes high geothermal gradients of 35 – 37 °C/km in the Flett sub-basin.
- "Cold" RHP model: upper crust heat production of Neoarchean metamorphic crust (1.6 $\mu W/m^3$). Moderate to good calibration of data on structural highs (e.g. Corona Ridge) but perhaps a more applicable lithospheric model for the basin areas with geothermal gradients of 28 – 34 °C/km in the Flett sub-basin.

The present-day architecture of the FSB predominantly results from Cretaceous continental rifting, most likely as three separate events during the early Cretaceous (145 – 130 Ma), Albian (110 – 100 Ma) and Campanian (85 – 80 Ma) (Iliffe *et al.,* 1999). Stretching (β) factors have been adjusted in each model to provide a cumulative β-factor consistent with the crustal thickness reported by Rippington *et al.* (2015) in each model location. For example, in the Flett sub-basin the crystalline crust (base sediment to top lithospheric mantle) may be as thin as 15 km, which assuming an initial, pre-rift crustal thickness of 40 km, infers a β-factor of *ca.* 2.7.

The thermal effects of these events are captured within the modelling, but the peak heat flow associated with the shallowing of the asthenosphere (1300 °C-isotherm) is significantly reduced by the deposition of fine clastic material associated with the rapid sedimentation rate (referred to as "sediment blanketing").

Quantifying igneous material

The methodology behind quantifying the thickness of Paleogene igneous intrusions is taken from Mark *et al.* (2018), where full details can be found.

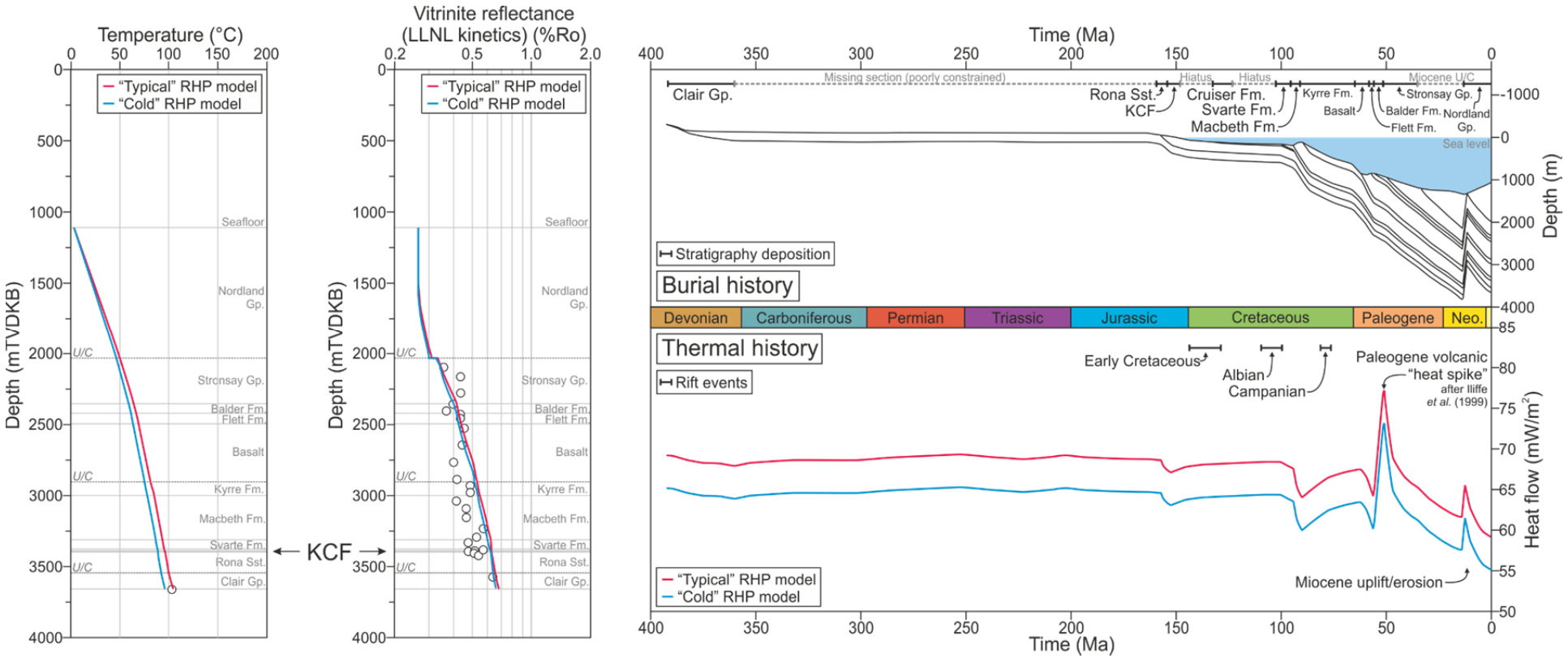

Example thermal calibration for well 213/27a-1Z (Rosebank field) to temperature and vitrinite reflectance data, comparing the effects of the "Typical" radiogenic heat production (RHP) model (akin to North Sea basement) compared to the "Cold" RHP model (based on the calculated RHP from basement samples in the FSB). Also shown is the burial history for the same well, highlighting the multiple Cretaceous rifting events and 800m of Miocene uplift/erosion inferred by the vitrinite reflectance data. The calculated heat flow history of the "Typical" RHP and "Cold" RHP models is derived from the lithospheric thickness through time in response to rift, volcanic and uplift events (which are kept consistent in both models) and the composition of the lithosphere (where only the RHP of the upper crust is adjusted).

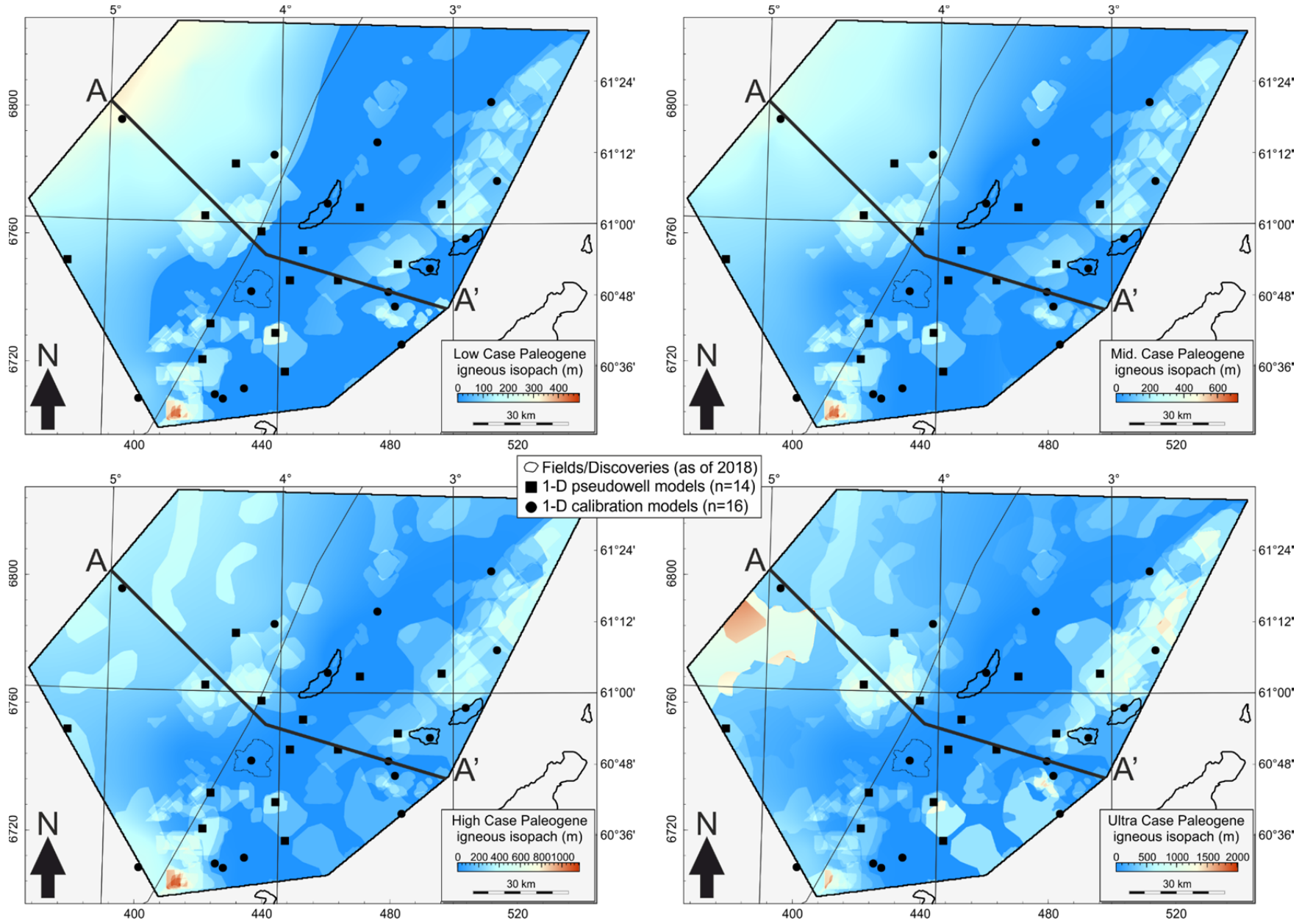

Low, Mid, High and Ultra Case igneous intrusion thickness scenarios (m) within the Upper Cretaceous across the AOI, after Mark *et al.* (2018). For this paper, the High Case scenario has been used in all scenarios which consider the presence or absence of Paleogene igneous intrusives. Data is provided by the University of Aberdeen.

					Igneous material not included (100% sediment)				Igneous material included (proportional to sill thickness)							
Pseudowell	Location	Depth to top KCF source rock (mTVDSS)	Igneous sill thickness (Mark *et al.*, 2018) (m)	Proportion of Cretaceous section (%)	Av. *k* of Cretaceous package (W/mK)	Surface heat flow (mW/m^2)	Average geothermal gradient (°C/km)	Onset of KCF oil expulsion (Ma)	Av. *k* of Cret. package (W/mK)	Surface heat flow (mW/m^2)	Average geothermal gradient (°C/km)	Onset of KCF oil expulsion (Ma)	Δ *k* of Cret. package (%)	Δ geothermal gradient (%)	Δ surface heat flow (%)	Δ timing of KCF oil expulsion (Myr)
1	JSB	8,294	744	17.5	2.01	54.1	29.2	97	2.45	53.7	28.1	84	17.86	-3.8	-0.7	13.0
2	JSB	6,559	522	19.9	1.88	56.9	30.9	76	2.38	56.3	30.3	69	20.89	-1.9	-1.1	7.0
3	JSB	7,049	98	3.9	1.90	56.9	31.4	77	2.00	56.6	30.8	71	4.84	-1.9	-0.5	6.0
4	JSB	8,123	666	18.4	1.80	54.1	30.3	123	2.26	53.8	28.5	110	20.36	-5.9	-0.6	13.0
5	JSB	9,141	1,190	43.4	1.92	52.3	28.3	91	3.01	51.1	26.1	74	36.11	-7.8	-2.3	17.0
6	FSB	8,212	0	0.0	1.86	52.7	28.9	110	1.86	52.7	28.9	110	0.00	0.0	0.0	0.0
7	FSB	6,877	316	10.5	1.89	54.4	30.5	81	2.15	53.9	29.7	72	12.17	-2.6	-0.9	9.0
8	CR	6,497	0	0.0	1.80	54.2	31.3	74	1.80	54.2	31.3	74	0.00	0.0	0.0	0.0
9	FSB	8,445	157	4.3	1.87	52.7	28.8	108	1.98	52.3	27.9	98	5.46	-3.1	-0.8	10.0
10	CR	6,819	100	3.1	1.92	54.1	28.0	81	2.00	53.9	27.9	78	3.82	-0.4	-0.4	3.0
11	FSB	8,168	305	8.8	1.92	53.2	28.5	91	2.14	52.7	27.8	85	10.32	-2.5	-0.9	6.0
12	FSB	9,094	591	14.3	1.95	54.1	28.5	96	2.31	52.6	26.4	80	15.46	-7.4	-2.8	16.0
13	CR	6,107	81	2.9	1.82	56.3	32.9	78	1.89	56	32.1	71	3.85	-2.4	-0.5	7.0
14	CR	5,704	775	32.7	1.81	56.4	32.2	63	2.63	55.5	31	56	31.09	-3.7	-1.6	7.0

Summary of outputs from the 14 1-D pseudowell models comparing the predicted effects of including igneous intrusions on the thermal conductivity (*k*) of the Cretaceous package, average geothermal gradient from seafloor (4 °C) to base Kimmeridgian, the surface heat flow at present day and the onset of oil expulsion from the primary source rock, the Kimmeridgian to Berriasian Kimmeridge Clay Formation (KCF). Positive values represent an increase in the respective parameter when considering including igneous material. The increased thermal conductivity of the Cretaceous package when intrusions are included reduces geothermal gradient, but surface heat flow does not increase due to the loss of radiogenic heat production (RHP) from sediments, as the igneous lithology has an RHP of 0 $\mu W/m^3$ in this study based on default values in Genesis software and the mafic composition of basaltic intrusions in the Faroe Shetland Basin. Location abbreviations: CR = Corona Ridge; FSB = Flett sub-basin; JSB = Judd sub-basin.

						"Typical" RHP crustal model (including igneous intrusions)			"Cold" RHP crustal model (including igneous intrusions)					
Pseudowell	Location	Depth to top KCF source rock (mTVDSS)	Depth to basement (mTVDSS)	Crystalline crustal thickness (after Rippington *et al.,* 2015) (km)	Total crust thickness (crystalline + sediments) (km)	Surface heat flow (mW/m^2)	Average geothermal gradient (°C/km)	Onset of KCF oil expulsion (Ma)	Surface heat flow (mW/m^2)	Average geothermal gradient (°C/km)	Onset of KCF oil expulsion (Ma)	Δ surface heat flow (%)	Δ geothermal gradient (%)	Δ timing of KCF oil expulsion (Myr)
1	JSB	8,294	9,000	19.0	28.0	57.0	34.1	92	51.6	31.1	78	11.0	11.5	14.0
2	JSB	6,559	8,600	20.0	28.6	60.1	36.0	70	53.8	32.6	56	12.2	12.2	14.0
3	JSB	7,049	8,200	20.0	28.2	61.4	37.1	77	54.3	33.1	61	13.8	14.3	16.0
4	JSB	8,123	8,600	20.0	28.6	60.3	33.1	91	53.1	29.5	61	14.1	14.6	30.0
5	JSB	9,141	10,200	19.0	29.2	55.4	30.4	62	50.2	27.8	56	10.9	11.3	6.0
6	FSB	8,212	9,000	12.0	21.0	55.6	31.2	97	50.8	28.7	82	10.0	10.6	15.0
7	FSB	6,877	7,500	16.0	23.5	54.4	33.5	65	52.7	32.6	61	3.3	3.4	4.0
8	CR	6,497	6,800	16.0	22.8	59.7	38.1	78	53.5	34.4	64	12.1	12.5	14.0
9	FSB	8,445	8,700	12.0	20.7	51.7	29.4	83	48.3	27.6	61	7.5	7.9	22.0
10	CR	6,819	8,900	24.0	32.9	56.4	32.9	73	48.5	28.6	56	17.2	17.9	17.0
11	FSB	8,168	9,000	12.0	21.0	50.9	29.4	67	47.8	27.8	58	6.8	7.1	9.0
12	FSB	9,094	9,700	12.0	21.7	52.1	29.1	70	48.8	27.3	58	7.3	7.7	12.0
13	CR	6,107	6,900	18.0	24.9	60.3	38.2	80	54.1	34.5	61	12.0	12.4	19.0
14	CR	5,704	7,300	20.0	27.3	61.8	38.2	61	54.4	34.0	52	14.1	14.4	9.0

Summary of outputs from the 14 1-D pseudowell models comparing the predicted effects of reducing the radiogenic heat production (RHP) from "Typical" values of 2.8 $\mu W/m^3$ (from the North Sea) in comparison to "Cold" RHP values of 1.6 $\mu W/m^3$ (based on Neoarchean basement in the FSB). The crustal structure is consistent in both scenarios, with thicknesses for the upper and lower crust taken from Rippington *et al.* (2015). Location abbreviations: CR = Corona Ridge; FSB = Flett sub-basin; JSB = Judd sub-basin.

Additional inputs

Water-depth has been inputted based on eustatic sea level curves by Haq *et al.* (1987) and adjusted in each model to match the predicted tectonic subsidence in each well location based on the inputted subsidence history.

Supplementary references

Chambers, L., Darbyshire, F., Noble, S. & Ritchie, D. 2005. NW UK continental margin: chronology and isotope geochemistry. British Geological Survey commissioned report, CR/05/095.

Cloetingh, S., Keemst, P., Kooi, H. & Fanavoll, S. 1992. Intraplate stresses and the post-Cretaceous uplift and subsidence in northern Atlantic basins. Norsk Geologisk Tidsskrift, 72, 229-235.

Ellis, D. & Stoker, M.S. 2014. The Faroe–Shetland Basin: a regional perspective from the Paleocene to the present day and its relationship to the opening of the North Atlantic Ocean. Geological Society, London, Special Publications, 397, 11-31.

Finlay, 2019. Calculated radioactive heat production in the North Sea: new data for petroleum systems analysis. Celebrating the life of Chris Cornford (1948-2017): Petroleum Systems Analysis 'Science or Art?' London, 24-25th April 2019.

Haq, B. U., Hardenbol, J. & Vail, P. R. 1987. The chronology of fluctuating sea level since the Triassic. Science, 235, 1156-1167.

Hasterok, D. & Webb, J. 2017. On the radiogenic heat production of igneous rocks. Geoscience Frontiers, 8, 919-940.

Iliffe, J. E., Robertson, A. G., Ward, G. H. F., Wynn, C., Pead, S. D. M. & Cameron, M. 1999. The importance of fluid pressures and migration to the hydrocarbon prospectivity of the Faeroe-Shetland White Zone. In: Fleet, A. J. & Boldy, S. A. R. (eds.) Petroleum Geology of Northwest Europe: Proceedings of the 5th Conference on the Petroleum Geology of Northwest Europe. The Geological Society, London.

Khutorskoi, M. D & Polyak, B. D. 2016. Role of radiogenic heat generation in surface heat flow formation. Geotectonics, 50, 179-195.

Larter, S., Huang, H., Adams, J., Bennett, B. & Snowdon, L. R. 2012. A practical biodegradation scale for use in reservoir geochemical studies of biodegraded oils. Organic Geochemistry, 45, 66-76.

Mark, N., Schofield, N., Gardiner, D., Holt, L., Grove, C., Watson, D., Alexander, A. & Poore, H. 2018. "Overthickening" of Sedimentary Sequences by Igneous Intrusions' Journal of the Geological Society.

Pepper, A. S. & Corvi, P. J. 1995. Simple kinetic models of petroleum formation Part 1: oil and gas generation from kerogen. Marine and Petroleum Geology, 12, 291-321.

Rateau, R., Schofield, N. & Smith, M. 2013. The potential role of igneous intrusions on hydrocarbon migration, West of Shetland. Petroleum Geoscience, 19, 259-272.

Rippington, S., Mazur, S. & Warner, J. 2015. The crustal architecture of the Faroe–Shetland Basin: insights from a newly merged gravity and magnetic dataset. Geological Society, London, Special Publications, 421, 169-196.

Rybach, L. 1988. Determination of heat production rate. In: Hänel, R., Rybach, L. & Stagena, L. (eds.) Handbook of Terrestrial Heat Flow Density Determination. Kluwer, Dordrecht, 125-142.

Schofield, N., Holford, S., Millett, J., Brown, D., Jolley, D., Passey, S.R., Muirhead, D., Grove, C., Magee, C., Murray, J., Hole, M., Jackson, C.A.L. & Stevenson, C. 2015. Regional magma plumbing and emplacement mechanisms of the Faroe-Shetland Sill Complex: implications for magma transport and petroleum systems within sedimentary basins. Basin Research, 29, 41-63.

Senger, K., Millett, J., Planke, S., Ogata, K., Eide, C., Festøy, M., Galland, O. & Jerram, D. 2017. Effects of igneous intrusions on the petroleum system: a review. First Break, 35, 47-56.

Turcotte, D. & Schubert, G. 2014. Geodynamics. 3rd edn. Cambridge: Cambridge University Press.

Databases

Applied Petroleum Technology (APT) Ltd., 2017. Geochemical evaluation of oil provenance & quality, West of Shetlands. Provided by the UK Oil & Gas Authority (OGA).

Chemostrat Inc., West of Shetland regional study (multi-client). Provided by Chemostrat.

IGI/GHGeochem, 2017. UK oils geochemical database (multi-client). Provided by IGI Ltd.

Intertek, 2006. Geochemical data of oil from the well 204/10-2.